



DESIGN OF A FUZZY CONTROLLER FOR COMPARISONS OF INDUCTION GENERATOR WIND POWER SYSTEMS

SWETHA A

PG scholar, Balaji institute of Technology & Science, JNTUH, Warangal, Telangana, India

MD ERSHAD ALI

M.Tech, Asst. Professor, Balaji Institute of Technology & Science JNTUH, Warangal, Telangana, India

ABSTRACT- This paper presents the performance comparison of fuzzy logic controlled wind power systems based on two different induction generators wind turbine simulator for the maximum power extraction. The two induction machines studied for the comparison are the squirrel-cage induction generator (SCIG) and the doubly fed induction generator (DFIG). The techniques of direct grid integration, independent power control, and the droop phenomenon of distribution line are studied and compared between the SCIG and DFIG systems with fuzzy. Both systems are modeled in MATLAB/SIMULINK environment, and the operation is tested for the wind turbine maximum power extraction algorithm results.

INTRODUCTION

Wind energy is an important source of electrical energy in years to come. Its main advantages come from the fact of being a renewable and environmental-friendly energy. At the beginning it was cheap and very robust but the generated power quality was poor. Most of wind power installations were limited to a few hundreds kilowatts connected to distribution grids [1]. Wind turbines and farms grew in size and ratio from the few hundreds kilowatts to megawatts size. The increased rated power of wind farms to areas with good wind resources leads to a new problem approach – to which extent the wind power interferes to the power system. The increasing emphasis on renewable wind energy has given rise to augmented attention on more reliable and advantageous electrical generator systems. Induction generator systems have been widely used and studied in wind power system because of their advantages over synchronous generators, such as smaller size, lower cost, and lower requirement of maintenance [1], [2]. The straightforward power conversion technique using squirrel-cage induction generator (SCIG) is widely accepted in fixed-speed applications with less emphasis on the high efficiency and control of power flow. However, such direct connection

with grid would allow the speed to vary in a very narrow range and thus limit the wind turbine utilization and power output. Another major problem with SCIG power system is the source of reactive power; that is, an external reactive power compensator is required to hold the distribution line voltage and prevent the whole system from overload. On the other hand, the doubly fed induction generator (DFIG) with variable-speed ability has higher energy capture efficiency and improved power quality and thus has attracted more attentions. With the advent of power electronic techniques, a back-to-back converter, which consists of two bidirectional converters and a dc link, acts as an optimal operation tracking interface between generator and grid [3]–[5]. Field-oriented control (FOC) is applied to both rotor- and stator-side converters to achieve desirable control on voltage and power [6], [7]. Generally, the FOC has been presented based on DFIG mathematical equations only. However, a three-phase choke is commonly used to couple the stator-side converter into the grid. Therefore, this paper proposes the FOC schemes of stator-side converter involving the choke, and it turns out that both stator- and rotor side converter voltages consist of a current regulation part and a cross-coupling part.

First, this paper presents a simulation setup to emulate the wind turbine operation in torque control mode and thus to obtain a power operation curve for optimal power control. Second, the modeling and simulation of SCIG and DFIG wind systems are studied. Comparison between SCIG without static var compensator (STATCOM) and SCIG with STATCOM as well as DFIG system with fuzzy controller is clearly indicates difference in resulted distribution line voltage.

II. MODELING OF WIND TURBINE

Wind energy is extracted through wind turbine blades and then transferred by the gearbox and rotor hub to the mechanical energy in the shaft, which drives the generator to

convert the mechanical energy to electrical energy. The turbine model is based on the output power characteristics, expressed as [3], [8] — (1a)

————(1b)

Where P_m is the mechanical output power in watts, which depends on power performance coefficient C_p , air density ρ , turbine swept area A , and wind speed v_w . $(1/2) \cdot \rho A v_w^3$ is equal to the kinetic energy contained in the wind at a particular speed v_w . The performance coefficient $C_p(\lambda, \beta)$, which depends on tip speed ratio λ and blade pitch angle β , determines how much of the wind kinetic energy can be captured by the wind turbine system. A nonlinear model describes $C_p(\lambda, \beta)$ as [8]

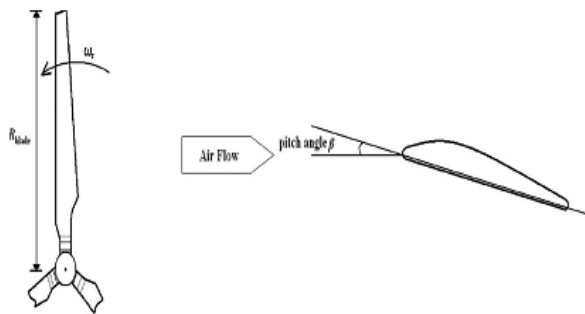


Fig.1: Schematics of turbine blade from different views

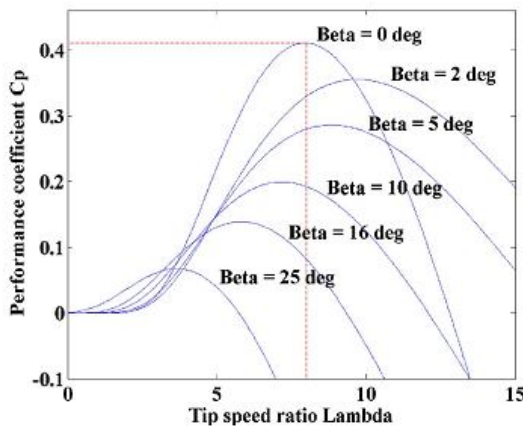


Fig.2: curve for the turbine model

(2)

Where $c_1=0.5$, $c_2= 116/\lambda_i$, $c_3=0.4$, $c_4=0$, $c_5=5$, $c_6=18/\lambda_i$, and — (3)

Where R_{blade} and ω_r are the blade radius and angular frequency of rotational turbine as depicted in Fig. 1. The

$C_p-\lambda$ curve for this particular turbine model at different β is shown in Fig. 2 where it is illustrated that, to achieve maximum C_p , one has $\beta=0^\circ$ and $\lambda=8$. The blade with fixed geometry will have fixed $C_p-\lambda$ characteristics, as described in (2) and (3). Therefore, to track the optimal output power, the curve of $P_m-\omega_r$ is the “map” to follow. In order to experimentally investigate the operation of wind turbine, a wind turbine emulator system is built to operate in torque control mode, using (1a)

————— (4)

Where C_m is the torque performance coefficient. It is dependent on ω_r , v_w , and β . Thus, based on turbine $C_p-\lambda$ model and by assuming $\beta=0^\circ$, the $C_m-\lambda$ curve is given in Fig. 3. At any particular v_w , one could obtain different torque and, thus, power output by varying rotor speed. The system configuration is shown in Fig. 4, where the ω_r is fed back to the controller for calculating C_m and, then, torque command.

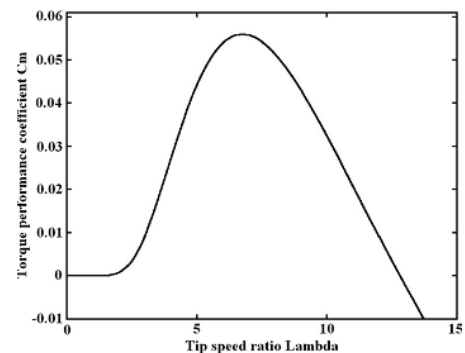


Fig.3: $C_m-\lambda$ curve for the turbine emulator.

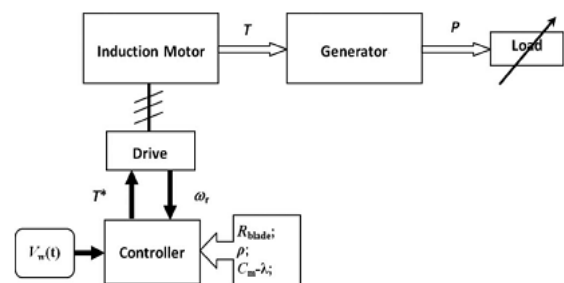


Fig. 4. Wind turbine emulator system.

III. DESCRIPTION OF SCIG

The schematics of the SCIG system Fig. 5 shows including the wind turbine, pitch control, and reactive power compensator. The entire system includes three stages for delivering the energy from wind turbine to the power grid.

The first one is wind farm stage which handles with low voltage V_{wt} , the second is distribution stage which has medium voltage V_{dis} , and the third is grid transmission stage which has high voltage V_{grid} . The three-phase transformers take care of the interface between stages [9]. As mentioned, nominal power P_{nSCIG} is considered as active power reference to regulate the pitch angle while V_{dis} and I_{dis} denote the distribution line-to-line voltage and phase current, and they are monitored to favor the reactive power compensation for distribution line. This fairly straightforward technique was first used since it is simple and has rugged construction, reliable operation, and low cost. However, the fixed-speed essential and potential voltage instability problems severely limit the operations of wind turbine [1], [3]. Since SCIG is of fixed-speed generator, for a particular wind speed, the output active power is fixed as well. Thus, with the increase of wind speed, so does the output power until the nominal power is reached. The wind speed at this moment is called nominal wind speed.

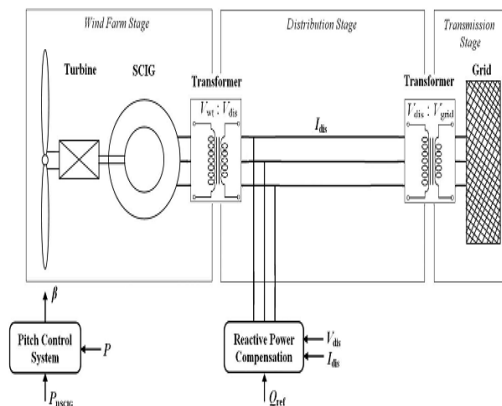


Fig. 5. SCIG wind power system topology.

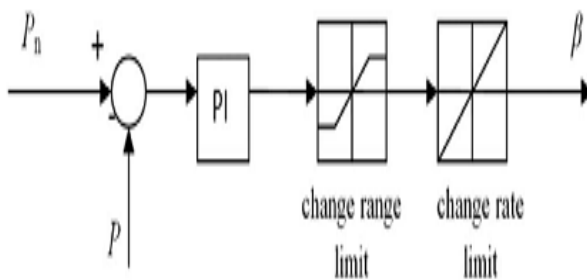


Fig. 6. Pitch angle control

Beyond this speed, the pitch angle system will prevent the output power from exceeding the nominal value. That is, when the wind speed is below nominal value, the power capture can vary with the change of wind speed; and when

the wind speed is above nominal value, the pitch angle control system will limit the generated power by changing the pitch angle. In such way, the output power will be stabilized at nominal value where the wind speed is always above nominal speed. The pitch angle is determined by an open loop control of regulated output active power and by that shown in Fig. 6. Due to the huge size of blade and, thus, inertia, pitch angle has to change in a slow rate and a reasonable range. It is also worthy to notice that, without reactive power source, in Section V, the SCIG system tends to lead to a voltage droop in distribution line which will cause overload problem. In the simulation section, the comparison between SCIG system with and without STATCOM is conducted.

IV. DESCRIPTION OF DFIG WINDPOWER SYSTEM

Traditionally, the dynamic slip control is employed to fulfill the variable-speed operation in wind turbine system, in which the rotor windings are connected to variable resistor and control the slip by the varied resistance [3], [10]. This type of system can achieve limited variations of generator speed, but external reactive power source is still necessary. Consequently, to completely remove the reactive power compensation and to control both active and reactive power independently, DFIG wind power system is one of most popular methods in wind energy applications [1], [3], [7]. This paper reproduces DFIG model first of all and then concentrates on the controlling schemes of power converters, in which the active and reactive power are controlled independently. In particular, the stator-side converter involving an RL series choke is proposed. Both controlling of rotor- and stator-side converter voltages end up with a current regulation part and a cross-coupling part. The wind turbine driving DFIG wind power system consists of a wound-rotor induction generator and an ac/dc/ac insulated gate bipolar transistor (IGBT)-based pulse width-modulated (PWM) converter (back-to-back converter with capacitor dc link), as shown in Fig. 7. In this configuration, the back-to-back converter consists of two parts: the stator-/grid-side converter and the rotor-side converter. Both are voltage source converters using IGBTs, while a capacitor between two converters acts as a dc voltage source. The generator stator windings are connected directly to grid (with fixed voltage and frequency of grid) while

the rotor winding is fed by rotor-side converter through slip rings and brushes, at variable frequency. The control system is divided into two parts—stator-side converter control system and rotor-side converter control system. An equivalent circuit of DFIG is depicted in Fig. 8, and the relation equations for voltage V , current I , flux Ψ , and torque T_e involve [4], [11], [12] are:

$$\frac{d\Psi_{ds}}{dt} = V_{ds} - R_s I_{ds} - \omega_s \Psi_{qs} \quad (5)$$

$$\frac{d\Psi_{qs}}{dt} = V_{qs} + \omega_s \Psi_{ds} \quad (6)$$

$$\frac{d\Psi_{dr}}{dt} = V_{dr} - R_r I_{dr} - s\omega_s \Psi_{qr} \quad (7)$$

$$\frac{d\Psi_{qr}}{dt} = V_{qr} + s\omega_s \Psi_{dr} \quad (8)$$

Where $L_s = L_{ls} + L_m$; $L_r = L_{lr} + L_m$; $s\omega_s = \omega_s - \omega_r$ represents the difference between synchronous speed and rotor speed; subscript sr, s, d, and q denote the rotor, stator, d-axis, and q-axis components, respectively; T_e is electromagnetic torque; and L_m , n_p , and J are generator mutual inductance, the number of pole pairs, and the inertia coefficient, respectively.

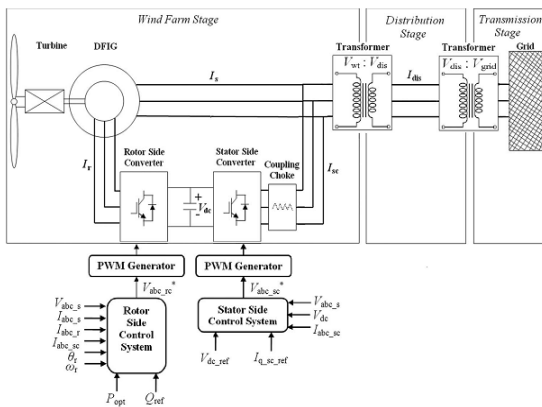


Fig. 7. Wind turbine–doubly fed induction generator system configuration.

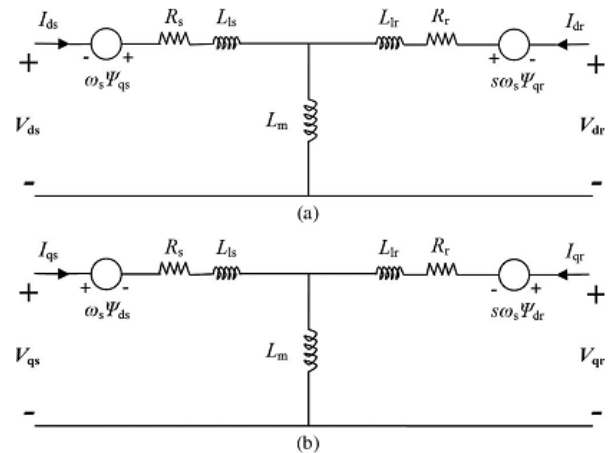


Fig. 8. Equivalent circuit of DFIG. (a)d-axis model. (b)q-axis model.

V. PROPOSED CONTROL STRATEGY

A. ROTOR-SIDE CONVERTER CONTROL

If the derivative parts in (5) are neglected, one can obtain stator flux as

$$\Psi_s = \frac{V_{ds}}{\omega_s} \quad (10)$$

Because of being directly connected to the grid, the stator voltage shares constant magnitude and frequency of the grid. One could make the d-axis align with stator voltage vector; it is true that $V_s = V_{ds}$ and $V_{qs} = 0$, thus $\Psi_s = \Psi_{qs}$ and $\Psi_{ds} = 0$, which is of stator-voltage-oriented vector control scheme, as depicted in Fig. 9. According to (7)–(9), the rotor-side converter reference current is derived as

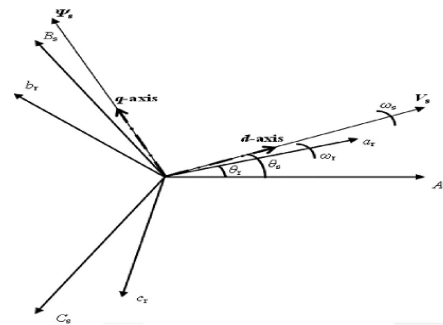


Fig. 9. Stator voltage FOC reference frame.

$$(11)$$

Where

$$(12)$$

Where I_{sc} , R_c , and F_{arc} are stator-side converter current, choke resistance, and friction factor, respectively. P_{opt} , P_{e_ref} , and P_{loss} are desired optimal output active power, reference active power, and system power loss. Combining (10)–(12), the active power is used as command inputs to determine current reference I_{dr_ref} . Meanwhile, the output reactive power is the stator reactive output power since the stator-side converter's reactive power is set to be zero. Then, one has

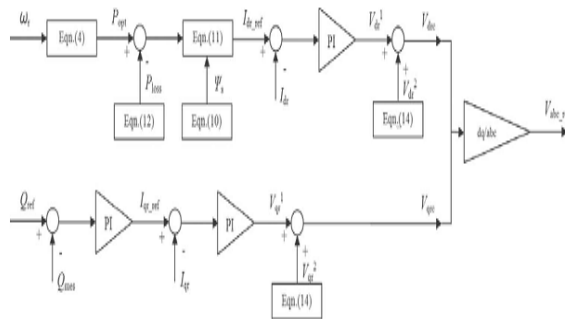


Fig. 10. Rotor-side converter control scheme.

$$(13)$$

Thus, the regulation of reactive power can lead to I_{qr_ref} , and then, the rotor-side converter voltage signals V_{d1} and V_{q1} are derived by the regulation of currents. In addition, the feed forward coupling parts V_{dc}^2 and V_q^2 are derived based on (6) and (8), as

$$\begin{aligned} &) \\ &)(14) \end{aligned}$$

Where the superscripts 1 and 2 denote the current regulation part and cross-coupling part, respectively. At last, rotor-side converter voltage signals in dq-axes are expressed as

$$(15)$$

where subscript rc denotes the rotor-side converter. After the conversion of dq-abc, the rotor-side converter voltage V_{abc_rc} can be obtained. Fig. 10 exhibits the control scheme for the aforementioned procedure.

B. STATOR-SIDE CONVERTER CONTROL

Concerning the use of three-phase series RL choke between stator- and stator-side converter, a cross-coupling model is required to derive the voltage signal of stator-side converter, as described in Fig. 11

$$(16)$$

Where the subscripts sc and ch denote the variables of stator side converter and choke. The coupling part of voltage signals V_{dsc} and V_{qsc} is expressed as

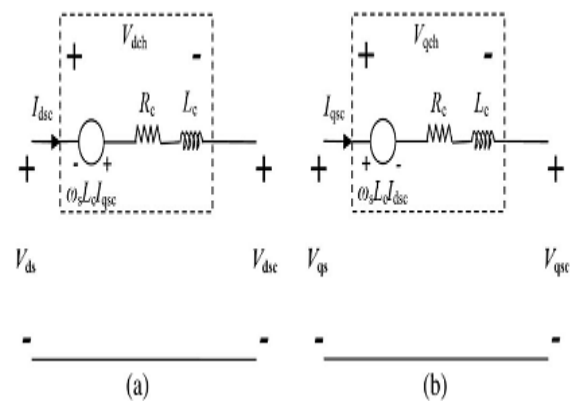


Fig. 11. Equivalent circuit of stator-side-converter choke. (a)d-axis model.(b)q-axis model.

$$(17)$$

More over V_{dch} and V_{qch} are determined by the regulation of currents I_{dsc} and I_{qsc} in which the current reference I_{qsc_ref} is given directly while I_{dsc_ref} is determined by the regulation of dc-link voltage V_{dc} . Thus, above all, the stator-side converter voltage signals V_{dsc} and V_{qsc} are obtained as follows and depicted in Fig. 12:

$$(15)$$

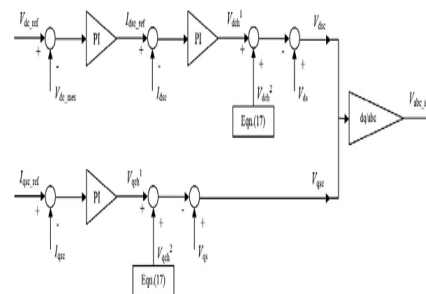


Fig. 12. Stator-side converter control scheme.

C. FUZZY LOGIC CONTROL:

In FLC, basic control action is determined by a set of linguistic rules. These rules are determined by the system. Since the numerical variables are converted into linguistic variables, mathematical modeling of the system is not required in FC. The FLC comprises of three parts: fuzzification, inference engine and defuzzification. The FC is characterized as; i.seven fuzzy sets for each input and output. ii.Triangular membership functions for simplicity. iii.Fuzzification using continuous universe of discourse. iv. Implication using Mamdani “s „min “ operator. v. Defuzzification using the „height“ method.

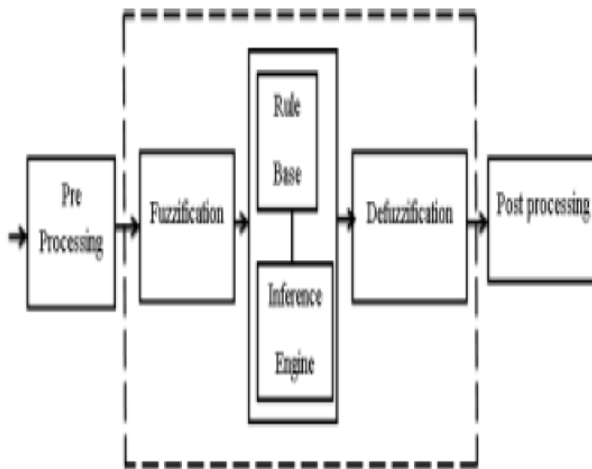


Fig 13.Fuzzy Logic Controller

	NB	NM	NS	ZE	PS	PM	PB
NB	NB	NB	NB	NB	NM	NS	ZE
NM	NB	NB	NB	NM	NS	ZE	PS
NS	NB	NB	NM	NS	ZE	PS	PM
ZE	NB	NM	NS	ZE	PS	PM	PB
PS	NM	NS	ZE	PS	PM	PB	PB
PM	NS	ZE	PS	PM	PB	PB	PB
PB	ZE	PS	PM	PB	PB	PB	PB

. FUZZY RULES

Fuzzification

Membership function values are assigned to the linguistic variables, using seven fuzzy subsets: NB (Negative Big), NM(Negative Medium), NS (Negative

Small), ZE (Zero), PS (Positive Small), PM(Positive Medium) and PB (Positive Big). The partition of fuzzy subsets and the shape of membershipfunction adapt the shape up to appropriate system. The value of input error $E(k)$ and change in error $CE(k)$ are normalized by an input scaling factor [11]and[12].

In this system the input scaling factor has been designed such that input values are between -1 and+1. The triangular shape of the membership function of this arrangement presumes that for any particularinput there is only one dominant fuzzy subset. The input error $E(k)$ for the FLC is given as

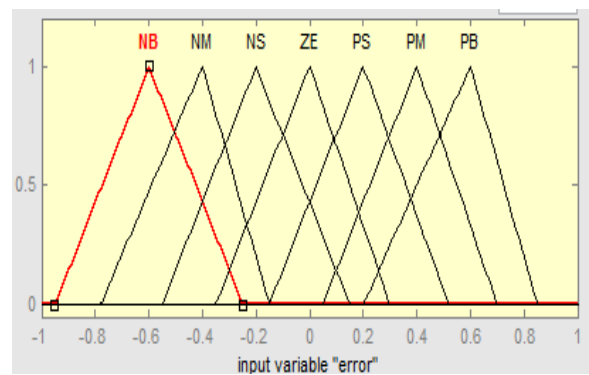


Fig. (a)

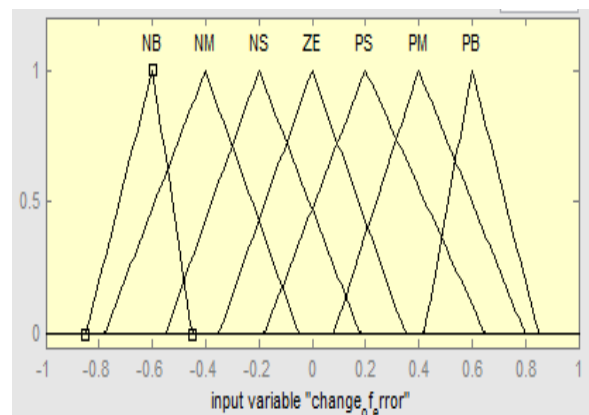


Fig.(b)

Fig.14 (a) &(b) Membership functions
Interference Method

Several composition methods such as Max–Min and Max-Dot have been proposed in the literature. In this paper Min method is used. The output membership function of

each rule is given by the minimum operator and maximum operator. Table 1 shows rule base of the FLC

Defuzzification

As a plant usually requires a non-fuzzy value of control, a defuzzification stage is needed. To compute the output of the FLC, „height“ method is used and the FLC output modifies the control output. Further, the output of FLC controls the switch in the inverter.. In order to control these parameters, they are sensed and compared with the reference values. To achieve this, the membership functions of FC are: error, change in error and output as shown in Figs.14(a), (b). In the present work, for fuzzification, non-uniform fuzzifier has been used. If the exact values of error and change in error are small, they are divided conversely and if the values are large, they are divided coarsely.

Where α is self-adjustable factor which can regulate the whole operation. E is the error of the system, C is the change in error and u is the control variable. A large value of error E indicates that given system is not in the balanced state. If the system is unbalanced, the controller should enlarge its control variables to balance the system as early as possible. On the other hand, small value of the error E indicates that the system is near to balanced state. Overshoot plays an important role in the system stability. Less overshoot is required for system stability and in restraining oscillations. C in (12) plays an important role, while the role of E is diminished. The optimization is done by α . The set of FC rules is made using Fig.14 is given in Table 1.

TABLE II
SCIG-BASED WIND POWER SYSTEM PARAMETERS

Parameter	value
Nominal Wind Speed	11 m/s
Nominal Active Power	0.855 MW
Grid Voltage	117 kV
Grid Frequency	60 Hz
Distribution Line Voltage	12.5 kV
Wind Turbine Bus Voltage	575 V
Stator Resistance	0.0048 p.u
Stator Leakage Inductance	0.1218 p.u.
Rotor Resistance	0.0044 p.u.
Rotor Leakage Inductance	0.1797 p.u.
Mutual Inductance	6.77 p.u.
STATCOM constant Voltage	4 kV
STATCOM Equivalent Capacitance C	625

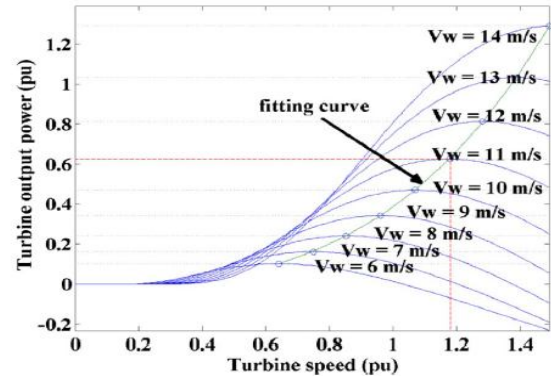


Fig. 15. Pm- ω curve for the turbine model.

VI. SIMULATION RESULTS

A. SCIG

A traditional SCIG wind power system is developed in MATLAB/SIMULINK, and the related system data used are given in Table II. In order to investigate the system performances, a ramp wind speed v_w is assumed that varies from $t=10$ to $t=16$ s and, then, it remains constant to the end of simulation $t=40$ s. Fig. 16(a)–(e) shows the dynamic variations and steady states of pitch angle β , generator speed ω_r , produced active power P, and consumed reactive power Q. First, the fluctuation in the results during $t=0$ to 2.5 s is due to the initial conditions. In the simulation, the initial speed of generator is set at slip $s=-0.01$ p.u. with respect to synchronous speed and, then, response to the wind speed input disturbance. Other initial values for power and voltages are zero.

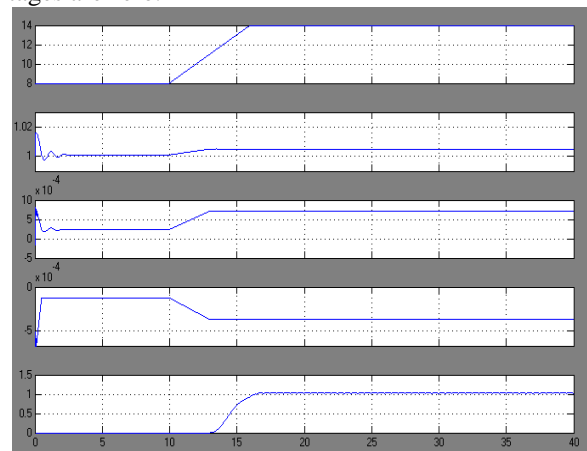


Fig. 16. Simulation results for SCIG system: (a) wind speed v_w ; (b) generator Speed ω_r ; (c) active power P; (d) reactive power Q; (e) pitch angle β .

The steady-state results for $v_w=8$ m/s indicate the operation points $\omega_r=1.0015$ p.u. and $P=0.29$ MW on Fig. 15. Since it is lower than nominal value of 0.855 MW, pitch angle control

is not working. After $t=10s$, with the increase of v_w , so do the ω_r and P until $t=13s$ when v_w exceeds the nominal value (11 m/s). This is because the pitch control is triggered to limit the increase of output power P and Q as shown in Fig. 16(b)–(d). In this way, the pitch control effectively limits the output P around the nominal value of 0.855 MW and settles a new pitch angle at roughly $t=17s$. This nominal operation point can also be observed in Fig. 15 ($v_w=11m/s; P=0.855MW; \omega_r=1.005p.u.$). It is noted that the rotor speed can only vary in very small scope around 1 p.u. (fixed-speed system) and, thus, impossible to achieve optimal active power output. Thus, the active power outputs at $v_w=8m/s$ and $\geq 11 m/s$ in SCIG are 0.29 and 0.855 MW which are lower than those in later DFIG system. Also, without independent control ability, SCIG system consumes reactive power of 0.41 Mvar in the steady state, which will lead to line voltage droop.

To provide necessary reactive power, a STATCOM is added on the distribution line to investigate the improvement. As in Fig. 17, distribution line voltage can drop by approximately 0.055 p.u. in SCIG system without STATCOM, which will be a potential induction of overload in system. In contrast, SCIG system with STATCOM can hold distribution voltage to 0.99 p.u. and favorable to grid system stability.

The compensated reactive power from STATCOM is shown in Fig. 18 and is equal to 0.3 Mvar in the steady state, a little bit less than the real consumed value in Fig. 16(d). Although STATCOM provides impressive help on constant distribution line voltage, the DFIG presents better result and does not need the help from STATCOM, as shown in Fig. 17.

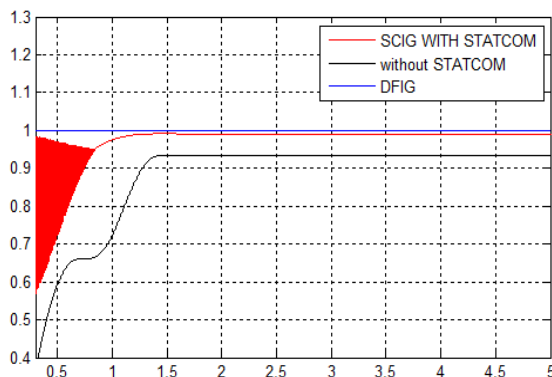


Fig. 17. Distribution voltages for SCIG system with/without STATCOM and DFIG system.

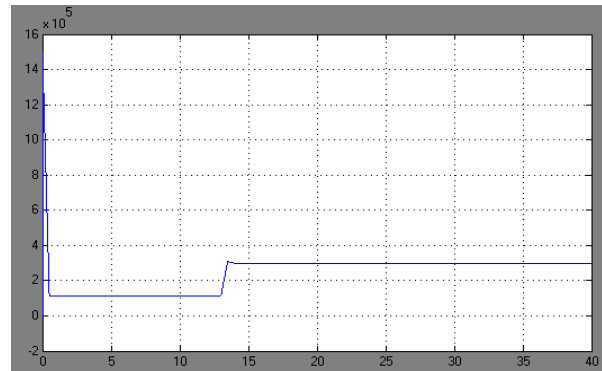


Fig. 18. STATCOM compensated reactive power.

B. DFIG with FUZZY:

By using the proposed optimal power curve as well as the system parameters listed in Table III, the DFIG wind power system is simulated with fuzzy. The DFIG with fuzzy system allows the optimal (maximum) output power operation in the absence of reactive power source. Also, the independent control of active and reactive power is achieved. In the MATLAB/SIMULINK model, the converter switch frequency is set to be 27 times the grid frequency f . To achieve acceptable accuracy, the power circuit and the control circuit models are discretized at different time steps. It is worthy to note that the nominal apparent power and nominal active power are considered as nominal electrical power and nominal mechanical power in this wind power system [3], [13]. Simulation and control system parameters are listed in Table IV and are preloaded into workspace before running the simulation and easy to be modified in m-file. First of all, the steady-state results of the system are shown in Fig. 19(a)–(d), where four wind speed cases $v_w= 7,9,10,$ and $12m/s$ to verify the optimal power output tracking are presented. All of them kept the bus voltage at 1170 Vdc, indicating the well operation of stator-side converter, while the reactive power is set to be zero as the input command. In order to track the optimal active power output, optimal rotor speeds are implemented accordingly. For instance, one could recall in

TABLE IV
SIMULATION AND CONTROL PARAMETERS

Parameter	value
Power System Sampling Period	5e-6 sec
Control System Sampling Period	1e-6 sec
Switch Frequency	1617 Hz
Transmission Distance	30 km
Reactive Power Regulator Coefficients	0.05;5 ;
DC-link Voltage Regulator Coefficients	0.002; 0.1 ;
Rotor-Side Current Regulator Coefficients	0.3; 8 ;
Stator- Side Current Regulator Coefficients	2.5 ; 500 ;

TABLE III
DFIG-BASED WIND POWER SYSTEM PARAMETERS

Parameter	Value
Nominal wind speed	11 m/s
Nominal apparent power	1.67 MVA
Nominal active power	1.5 MW
Power factor pf	0.9
Grid voltage	117 kV
Grid frequency f	60 Hz
Distribution line voltage	12.5 kV
Wind turbine bus voltage	575 V
Generator number of pole pairs	3
Stator resistance	0.0071 p.u.
Stator leakage inductance	0.171 p.u.
Referred rotor resistance	0.005 p.u.
Referred rotor leakage inductance	0.156 p.u.
Stator-to-Grid coupling resistance	0.003 p.u.
Stator-to-Grid coupling inductance	0.3 p.u.
Mutual inductance	2.9 p.u.
Nominal Dc-link voltage	1.2 kV
DC-link capacitance C	10 mF
Maximum C converter current	0.5 p.u.
System inertia coefficient H	5 second
Generator friction damping F	0.01 p.u.

It is noticed that P and Q are vanished during the first cycle (1/60 s) in displayed result because of the calculation time cost. Second, the system dynamic response to varied wind speeds is investigated. Due to the large H of the system, dynamic variation can last and be observed in a long time period before converging to the steady-state values. To shorten such period, H= 0.1s is used in this part of simulation. With stable steady-state initial values, three regular types of wind speeds are examined for dynamic responses, including step, ramp, and gusty winds. The varied winds and corresponding results for V_{dc}, P, and Q are shown in Figs. 20 and 21, where the system can always reach a new optimal steady state after a few seconds. In the aforementioned results, the reduced inertia constants can only decrease the converging time, making the system reach a new steady state quicker, and it has no effects on steady-state values. At last, the system dynamic response to a grid disturbance is investigated. At $v = 9\text{m/s}$, a remote voltage drop in grid is programmed from $t=0.09\text{ to }0.29\text{ s}$.

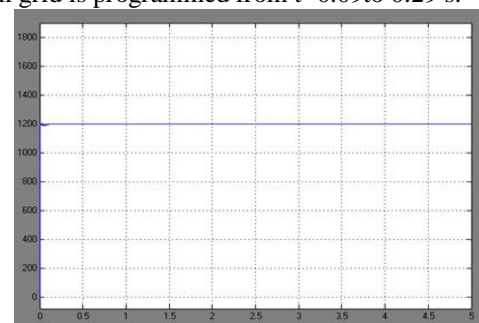
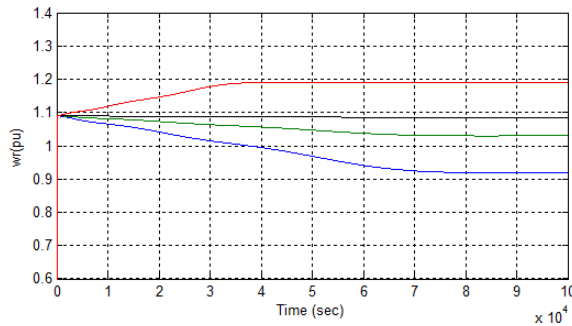
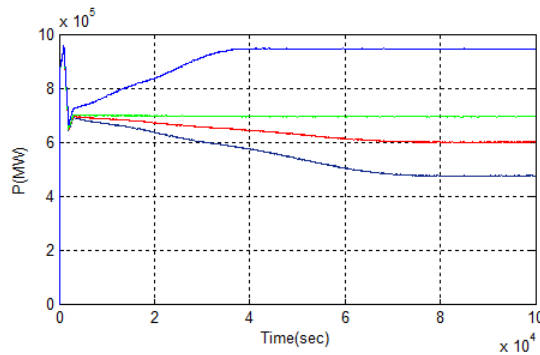


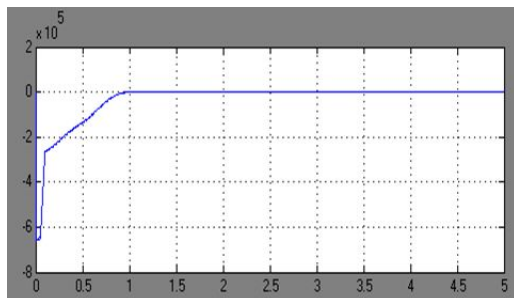
Fig. 15 that, at $v = 7\text{m/s}$, the optimal output active power is 0.17 p.u. with nominal power of 1.5 MW, i.e., 0.255 MW. A little bit power droop could be observed from simulation results which are caused by power loss in (12). Meanwhile, the optimal rotor speed is also achieved at 0.75 p.u., same as the value in Fig. 15. Similarly, the optimal trackings of output power and rotor speed are exhibited in other wind speed cases as well. Therefore, it can be concluded that the system works well to follow the optimal Power control at steady-state operation.



(b)



(c)



(d)

Fig. 19. System responses to different constant wind speeds. (a) DC-link voltage Vdc.(b) Rotor speed ω_r . (c) Active power (d) Reactive power Q.

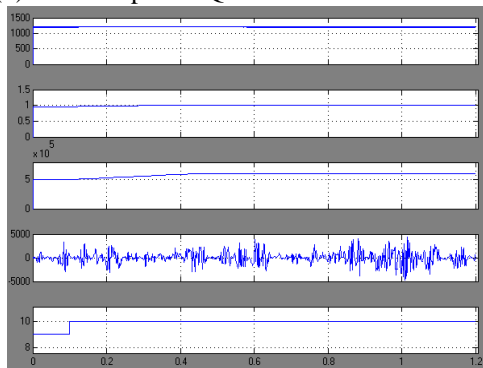


Fig. 20. Wind step response. (a) DC-link voltage Vdc. (b) Rotor speed ω_r . (c) Active power P. (d) Reactive power Q. (e) Wind speed v_w .

The dynamic responses are presented in Fig. 21. During this process, since the wind speed remains the same, control system effectively makes the system recovers in approximate 0.1 s. D. Comparison Between Two Systems A summary of SCIG and DFIG systems is presented in Table V based on research of this paper. The comparison shows the superiority of DFIG system over SCIG system in terms of efficiency, controllability, and high-power applications. Also, the higher cost of slip rings and power electronics can be compensated by more power output.

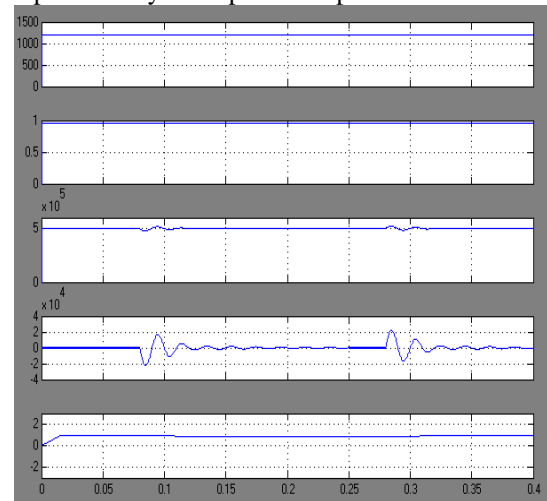


Fig. 21. Dynamic responses to grid voltage droop. (a) DC-link voltage Vdc. (b) Rotor speed ω_r . (c) Active power P. (d) Reactive power Q. (e) Grid voltage v_{grid} .

TABLE V
SUMMARY OF SCIG AND DFIG WIND POWER SYSTEMS

	SCIG	DFIG
Speed Operation	Fixed or limited variable	Variable
Line Voltage	Drop by 0.05 p.u.	Stable constant
Control Scheme	Pitch control	FOC
Active Power	Varies with but not optimally	Varies with optimally

1980.

Reactive Power	Uncontrollable; need compensation	controllable
Power Rating	<1 MW	>1MW
Cost and Complexity	Low and simple	high

CONCLUSION

This paper proposes the performance comparison of fuzzy logic controlled wind power systems. This paper has presented the comparison of the wind turbine systems using SCIG and DFIG generator systems. A SCIG and a DFIG with fuzzy wind power systems are modeled and simulated in Mat lab/Simulink. The SCIG system presents the need of external reactive power source to support grid voltage, and it can keep the output power at the nominal level by pitch control but cannot accordingly change the rotor speed to achieve maximum wind power capture at different wind speeds. In contrast, the DFIG with fuzzy system does not need reactive power compensator to hold distribution line voltage and achieves optimal active power controlling. Both voltage control schemes for two converters consist of a current regulation part and a cross-coupling part. The turbine emulator system performs well and follows the theoretical and simulated maximum power extraction points in different operating conditions.

REFERENCES

[1] M. Orabi, T. Ahmed, and M. Nakaoka, "Efficient performances of induction generator for wind energy utilization," in Proc. 30th Annu. Conf. IEEE Ind. Elect. Soc., Nov. 1704, pp. 838–843.

[2] M. Molinas, J. A. Suul, and T. Undeland, "Low voltage ride through of wind farms with cage generators: STATCOM versus SVC," IEEE Trans. Power Electron., vol. 20, no. 3, pp. 1104–1117, May 1708.

[3] Z. Chen, J. M. Guerrero, and F. Blaabjerg, "A review of the state of the art of power electronics for wind turbines," IEEE Trans. Power Electron., vol. 21, no. 8, pp. 1559–1575, Aug. 1709.

[4] Y. Lei, A. Mullane, and G. Light body, "Modeling of the wind turbine with a doubly fed induction generator for grid integration studies," IEEE Trans. Energy Convers., vol. 18, no. 1, pp. 257–264, Mar. 1706.

IEEE Int. Conf. Mechatron. Autom., Aug. 1709, pp. 1976

[5] R. Ganon, G. Sybille, and S. Bernard, "Modeling and real-time simulation of a doubly-fed induction generator driven by a wind turbine," presented at the Int. Conf. Power Systems Transients, Montreal, QC, Canada, Jun. 1705, Paper IPST05-162.

[6] H. Sun, Y. Ren, and H. Li, "DFIG wind power generation based on back-to-back PWM converter," in Proc.

[7] L. Xu and P. Cartwright, "Direct active and reactive power control of DFIG for wind energy generation," IEEE Trans. Energy Convers., vol. 18, no. 3, pp. 750–758, Sep. 1706.

[8] S. Heier, Grid Integration of Wind Energy Conversion Systems. Hoboken, NJ, USA: Wiley, 1706.

[9] N. W. Miller, W. W. Price, and J. J. Sanchez-Gasca, "Dynamic modeling of GE 1.5 And 3.6 wind turbine-generators," GE Power Systems Energy Consulting, Gen. Elect. Int., Inc., Schenectady, NY, USA, Oct. 1703.

[10] R. Pena, J. C. Clare, and G. M. Asher, "Doubly fed induction generator using back-to-back PWM converters and its application to variable-speed wind energy generation," Proc. Inst. Elect. Eng.—Elect. Power Appl., vol. 143, no. 3, pp. 201–211, May 1696.

[11] Feijoo, J. Cidras, and C. Carrillo, "Third order model for the doubly-fed induction machine," Elect. Power Syst. Res., vol. 56, no. 2, pp. 118–127, Nov. 1700.

[12] T. Ghennam, E. M. Berkouk, and B. Francois, "DC-link voltage balancing algorithm using a space-vector hysteresis current control for three-level VSI applied for wind conversion system," in Proc. Power Elect. Appl. Eur. Conf., Sep. 1707, pp. 1–10.

[13] M. Stiebler, Wind Energy Systems for Electric Power Generation. Berlin, Germany: Springer-Verlag, 1708.

SWETHA A currently pursuing her M.Tech in Electrical Power Systems in Balaji institute of Technology and Sciences, Warangal, Telangana, India affiliated to JNTU University, Hyderabad. She has done her B.Tech degree from Balaji Institute of Engineering and Sciences, affiliated to JNT University, Hyderabad, Telangana, India in 2011 and her fields of interest include Power Systems and Industrial Drives.

MD ERSHAD ALI has completed his M.Tech in Electrical Power Systems from Jayamukhi Institute of Science & Technology JNTUH, Telangana, India in 2013 and B.tech from Vagdevi College of Engineering in 2008. Presently working as Asst. Professor in Balaji Institute of Technology & Science from 2009 to till date. His fields of interest include Renewable Energy Sources and Industrial Drives.